Frontiers of Information Technology & Electronic Engineering
www.jzus.zju.edu.cn; engineering.cae.cn; www.springerlink.com
ISSN 2095-9184 (print); ISSN 2095-9230 (online)
E-mail: jzus@zju.edu.cn

Review:

Chip-based waveguides for high-sensitivity biosensing and super-resolution imaging*

Chen-lei PANG[1], Xu LIU[1], Wei CHEN[2,3], Qing YANG[†‡1,4]

[1]*State Key Laboratory of Modern Optical Instrumentation, College of Optical Science and Engineering, Zhejiang University, Hangzhou 310027, China*

[2]*Deparment of Cell Biology, Zhejiang University School of Medicine, Hangzhou 310058, China*

[3]*State Key Laboratory of Modern Optical Instrumentation, Collaborative Innovation Center for Diagnosis and Treatment of Infectious Diseases, Zhejiang University, Hangzhou 310058, China*

[4]*Collaborative Innovation Center of Extreme Optics, Shanxi University, Taiyuan 030006, China*

[†]E-mail: qingyang@zju.edu.cn

Received Apr. 24, 2019; Revision accepted Aug. 12, 2019; Crosschecked Mar. 3, 2020

Abstract: In this review, we introduce some chip-based waveguide biosensing and imaging techniques, which significantly reduce the complexity of the entire system. These techniques use a well-confined evanescent field to interact with the surrounding materials and achieve high sensitivity sensing and high signal-to-noise ratio (SNR) super-resolution imaging. The fabrication process of these chips is simple and compatible with conventional semiconductor fabrication methods, allowing high-yield production. Combined with recently developed chip-based light sources, these techniques offer the possibility of biosensing and super-resolution imaging based on integrated circuits.

Key words: Waveguide-based sensing; Waveguide-based imaging; Evanescent illumination; Frequency shifting and stitching
https://doi.org/10.1631/FITEE.1900211 **CLC number:** Q248; O438.2

1 Introduction

With the developments in biomedical research, healthcare, pharmaceuticals, and environmental monitoring, highly sensitive biosensors are needed for reliable analysis of DNA, RNA, proteins, and drugs. Super-resolution imaging is also needed to observe the biological interactions in microorganisms, cells, and tissues. In the past several years, numerous biosensor and micro/nanoscopy systems have been designed to meet these requirements.

The previously reported biodetection methods have involved the use of electrochemical (Millan et al., 1994; Zhang JJ and Li, 2004; Prakash et al., 2009), acoustic (Su et al., 1994; Watts et al., 1995), and optical sensors (Graham et al., 1992). In contrast to electrochemical and acoustic sensing, optical sensors are immune to electro-magnetic interference and can provide multiplexed detection. In particular, waveguide-based biosensors have effectively reduced the complexity of the detection systems, and some of them have been commercialized. Generally, these techniques can be divided into two groups, i.e., fluorescence-based sensing and label-free sensing. In

‡ Corresponding author

* Project supported by the National Natural Science Foundation of China (Nos. 61735017, 61822510, and 51672245), the Zhejiang Provincial Natural Science Foundation of China (No. R17F050003), the National Key Basic Research Program of China (No. 2015CB352003), the Fundamental Research Funds for the Central Universities, China, the Program for Zhejiang Leading Team of S&T Innovation, the Cao Guangbiao Advanced Technology Program, and the First-Class Universities and Academic Programs

ORCID: Chen-lei PANG, https://orcid.org/0000-0002-3167-9090; Qing YANG, https://orcid.org/0000-0001-5324-4832

fluorescence-based sensing, either the target molecules or biorecognition molecules are labeled with fluorescent tags; the fluorescence indicates the location of the interaction, and the corresponding fluorescence intensity demonstrates the strength of the interaction between the target and biorecognition molecules (Grandin et al., 2006; Moerner, 2007; Hassanzadeh et al., 2008; Agnarsson et al., 2009; Ramachandran et al., 2013). Since fluorescence labeling makes the interaction process visible, these techniques can also be called fluorescence-based imaging techniques. One drawback of these techniques is that the dynamics of the biomolecules may be affected by the labeled fluorescent molecules. Because of the scattering and absorption of fluorescent light by the surrounding materials, analyzing a fluorescence signal poses a challenge in quantitative analysis as well. In label-free sensing, no staining process is needed and the targets can be detected in their natural states. Recently, many label-free sensing techniques have been reported, including surface plasmon resonance (SPR) biosensors (Liedberg et al., 1983; Homola et al., 1999; Nikitin et al., 2000; Chung et al., 2006; Hastings et al., 2007; Hoa et al., 2007), waveguide based interferometer biosensors (Brandenburg, 1997; Lin VSY et al., 1997; Weisser et al., 1999; Ymeti et al., 2003), optical waveguide based biosensors (Goddard et al., 1994, 2002; Watts et al., 1994; Horváth et al., 2003), and waveguide based ring resonator biosensors (Serpengüzel et al., 1995; Hanumegowda et al., 2005; Noto et al., 2005; Teraoka and Arnold, 2006; Zhu et al., 2006; Suter et al., 2007; White et al., 2007; White and Fan, 2008). These techniques are designed with different structures, but they share the same working principle, i.e., measuring the refractive index (RI) change induced by ambient conditions.

The invention of the high-resolution optical microscope has opened the door to the microscopic world, allowing researchers to image and investigate microorganisms, cells, and tissues under living conditions. However, the spatial resolution of the classical optical microscopes has been limited to approximately half the wavelength of the light used, about 200–300 nm in the lateral direction and 500 nm in the axial direction. Due to the limitations of the spatial resolution, many biological interactions occurring at the level of the subcellular structures in the size ranges of tens to a few hundred nanometers cannot be resolved. In the past few years, a number of super-resolution microscopy techniques have been invented to overcome the diffraction barrier. According to their working mechanisms, these techniques can also be classified into two groups, i.e., fluorescent labeling microscopy by exploiting photo-switching of fluorescent probes or a nonlinear response in the fluorescence emission and label-free microscopy by capturing the high spatial frequency carried by the evanescent field. The first group includes stimulated emission depletion (STED) (Abbe, 1873; Klar et al., 2001; Willig et al., 2006), structured illumination microscopy (SIM) (Gustafsson, 2005; Gustafsson et al., 2008), stochastic optical reconstruction microscopy (STORM) (Bates et al., 2007; Schermelleh et al., 2010), photo-activated localization microscopy (PALM) (Betzig et al., 2006; Hess et al., 2006), and total internal reflection fluorescence microscopy (TIRFM) (Axelrod et al., 1983; Axelrod, 2001). The second group includes near-field scanning optical microscopy (NSOM) (Betzig and Trautman, 1992; Zenhausern et al., 1995; Hecht et al., 2000; Kim and Song, 2007; Rotenberg and Kuipers, 2014), hyperlens (Liu ZW et al., 2007; Rho et al., 2010; Sun et al., 2015; Lee et al., 2017), microsphere contact (Hao et al., 2011; Wang et al., 2011; Darafsheh et al., 2012), and nanowire ring illumination (Liu XW et al., 2017; Pang et al., 2017). These techniques have realized the resolution of previously unresolved details in cellular structures or nanostructures. In particular, fluorescence labeling techniques have achieved applications in modern cell diagnosis.

The above sensing and imaging techniques have promoted research in areas such as target analysis, drug development, and disease diagnostics; some of the techniques have already been commercialized. In this review, taking the complexity of the system, technical demands, and relative cost into account, we focus on waveguide-based sensing and imaging techniques. These waveguide-based techniques significantly reduce the complexity of the entire system. At the same time, the fabrication process for these waveguide chips is compatible with conventional semiconductor-fabrication methods, and thus the chips can be produced in high yields. These advantages make waveguide-based super-resolution sensing/imaging a promising candidate in future applications.

2 Principle and working mechanism

Generally, by fabricating a submicron-period grating patterned into the waveguide layer, light can be effectively coupled into the waveguide at a specific incident angle (Fig. 1a) (Zourob and Goddard, 2005; Liu Q et al., 2013). In addition, other methods such as end-fire coupling (Fig. 1b) and prism coupling are used in the coupling (Goddard et al., 1994, 2002; Watts et al., 1994). Grating couplers are easy to use, but they require a complex fabrication process and precise control of the incident angle. Since a mono-mode waveguide may be only 100–200 nm thick, precise control in coupling the optical fibers or objective lens is required for the end-fire coupling method. Prism coupling is easy to use, but it also requires care when setting up.

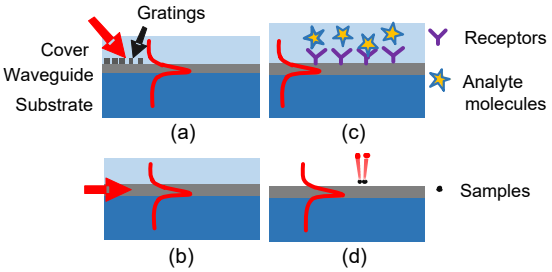

Fig. 1 Principle of evanescent field sensing and imaging: (a) in-coupling of light into the waveguide through a submicron-period grating pattern; (b) end-fire coupling of light into the waveguide; (c) schematic of waveguide-based biosensing; (d) schematic of waveguide-based super-resolution imaging

When light propagates in the waveguide, an exponentially decaying evanescent field in the direction perpendicular to the waveguide surface is generated. The penetration depth of the evanescent field extending into the cover layer is defined as the distance where the electric field amplitude has dropped to 1/e of its value at the surface, and can be given by (Agnarsson et al., 2009, 2015)

$$d=\frac{\lambda}{2\pi}\frac{1}{\sqrt{n_{\mathrm{eff}}^2-n_{\mathrm{c}}^2}}, \tag{1}$$

where $n_{\mathrm{eff}}=n_{\mathrm{w}}\sin\alpha$ is the effective index of the waveguide mode, n_{w} is the RI of the waveguide, α is the reflection angle at the interface between the waveguide and cover layers, and n_{c} represents the RI of the cover layer. The corresponding phase velocity of light within the waveguide is defined as $v_{\mathrm{p}}=c/n_{\mathrm{eff}}$, where c is the speed of light in a vacuum. The reflection angle α depends on the following parameters: the wavelength of incident light λ, refractive indexes of the different layers, thicknesses of different layers, and the polarization of light. The variation in each of these parameters will lead to the change in the effective index of the waveguide mode, and in turn in the wavelength of the guided light, causing a phase shift relative to the original state.

Generally, the thickness and RI of the cover layer are sensitive to ambient conditions and easy to use for detection of the adsorption/binding of any kind of chemical or biological molecule. Fig. 1c demonstrates a situation in which the target molecules are absorbed by the biorecognition molecules, forming a thin adlayer with an RI of n_{ad}, where n_{ad} represents the refractive index of the thin adlayer. The relationship between the effective mode index n_{eff} and the RI of the cover layer n_{c} satisfies the following equation:

$$\frac{\partial n_{\mathrm{eff}}}{\partial n_{\mathrm{c}}}=\frac{n_{\mathrm{c}}}{n_{\mathrm{eff}}}\cdot\frac{n_{\mathrm{w}}^2-n_{\mathrm{eff}}^2}{n_{\mathrm{w}}^2-n_{\mathrm{c}}^2}\cdot\frac{\Delta d_{\mathrm{c,s}}}{d_{\mathrm{eff}}}\left[2\left(\frac{n_{\mathrm{eff}}}{n_{\mathrm{c}}}\right)^2-1\right]^r, \tag{2}$$

where r=0 for the transverse electric (TE) mode and r=1 for the transverse magnetic (TM) mode. $d_{\mathrm{eff}}=d_{\mathrm{w}}+\Delta d_{\mathrm{c,s}}$ represents the effective waveguide thickness and depends on the polarization of the mode field. Here, d_{w} represents the thickness of waveguide and $\Delta d_{\mathrm{c,s}}$ includes the penetration depths of the evanescent field into the cover layer and substrate layer. The detailed calculation processes were described in Tiefenthaler and Lukosz (1989).

The evanescent field propagating in a planar waveguide can work as a light source with high wave vectors to tune the ON/OFF state of the labeled fluorescent molecules. As demonstrated in Fig. 1d, the evanescent field around the interface of the waveguide can directly interact with the sample as well. By shifting the high spatial frequency information of the sample into the passband of the microscope system, the subwavelength details in the sample can thus be resolved.

Under the illumination of a normally incident plane wave Ae^{ik_0z}, the scattering field from an object

$O(x, y)$ placed in the z=0 plane can be written as the superposition of a series of plane waves and evanescent waves (Liu XW et al., 2017):

$$\begin{aligned} &A\mathrm{e}^{\mathrm{i}k_0 z}O(x,y)\big|_{z=0} \\ &=\iint_{-\infty}^{+\infty}F(f_x,f_y)\exp\Big[\mathrm{i}(2\pi f_x x+2\pi f_y y \\ &+z\sqrt{k_0^2-(2\pi f_x)^2-(2\pi f_y)^2}\,)\Big]\mathrm{d}f_x\mathrm{d}f_y\big|_{z=0}. \end{aligned} \tag{3}$$

Herein k_0 is the wave vector of incident light in a vacuum. f_x and f_y represent the spatial frequencies of the object along the x and y directions, respectively. $F(f_x, f_y)\mathrm{d}f_x\mathrm{d}f_y$ is the weight function of each wave. λ is the wavelength of the illumination light. From Eq. (3), we can find the subwavelength details of samples carried by the high spatial frequency information, corresponding to $\left(2\pi f_x\right)^2+\left(2\pi f_y\right)^2>k_0^2$, which is blocked to be detected. To resolve the samples, an effective method is the shifting of the high spatial frequency information into the passband of the microscope system.

The propagation of an evanescence field can be written as

$$I(x,y)=A\exp[\mathrm{i}(k_{\mathrm{ex}}x+k_{\mathrm{ey}}y+k_{\mathrm{ez}}z)], \tag{4}$$

where k_{ex}, k_{ey}, and k_{ez} are the wave vectors of the evanescent field along the x, y, and z directions, respectively.

When an object $O(x, y)$ interacts with the evanescent waves in the z=0 plane, the scattering field can be given as

$$\begin{aligned} &I(x,y)O(x,y)\big|_{z=0} \\ &=\iint_{-\infty}^{+\infty}F(k_x,k_y)\exp\Big\{\mathrm{i}[(2\pi f_x+k_{\mathrm{ex}})x+(2\pi f_y+k_{\mathrm{ey}})y \\ &+z\sqrt{k_0^2-(2\pi f_x+k_{\mathrm{ex}})^2-(2\pi f_y+k_{\mathrm{ey}})^2}\,]\Big\}\mathrm{d}f_x\mathrm{d}f_y\big|_{z=0}. \end{aligned} \tag{5}$$

As demonstrated in Eq. (5), under an evanescent wave illumination, the high spatial frequency information of the sample around $(-k_{\mathrm{ex}}, -k_{\mathrm{ey}})$ with a radius of k_0 can propagate to the far field in the form of a propagating wave. Then the propagating waves would be collected by the microscope system and recorded by the CCD camera. Since the illumination light is an evanescent wave with $k_{\mathrm{e}}=2\pi n_{\mathrm{eff}}/\lambda$, the resolution of the system can be defined as (Pang et al., 2017)

$$R=\frac{2\pi}{k_{\mathrm{c}}+k_{\mathrm{e}}}=\frac{\lambda}{\mathrm{NA}+n_{\mathrm{eff}}}, \tag{6}$$

where $k_{\mathrm{c}}=k_{\mathrm{e}}=2\pi\mathrm{NA}/\lambda_0$ is the cut-off frequency of the microscope system, and NA is the numerical aperture of the objective. Because the effective mode index n_{eff} within the waveguide is usually larger than NA, the resolution of the system can thus be improved.

3 Chip-based optical waveguide biosensors

Waveguide-based (bio)chemical sensors share the same working mechanism. By coating a chemically selective layer on the surface, analyte molecules in the gaseous or liquid sample are absorbed. Hence, changes in the effective index of the TE and TM modes are induced. Generally, the effective index changes Δn_{eff} can be induced by three different situations: (1) the formation of a homogenous adlayer (formed by absorbed or bound molecules) with thickness of d_{F} and RI n_{F}, (2) changes to Δn_{c} in the RI of the cover layer or changes to Δd_{c} in the thickness of the cover layer, and (3) the adsorption of target molecules in the pores of the waveguide. As discussed above, the effective index n_{eff} gives the phase velocity v_{p}, and the changes in Δn_{eff} can thus be measured by many optical methods. Accordingly, these biosensors can be divided into different groups, such as optical waveguide based biosensors, interferometer-based biosensors, ring resonator based biosensors, and microcavity-based biosensors.

3.1 Optical waveguide based biosensors

Optical waveguide based biosensors, called resonant mirrors (RMs), have been proposed and developed for decades (Cush et al., 1993; Sundram et al., 1993; Goddard et al., 1994, 2002; Watts et al., 1994). In an RM design, with the help of a coupling grating or prism, light above the critical angle can be

coupled into the high index waveguide. Specifically, at the resonant angle, the incident light is strongly coupled into the waveguide, and a strong reflection can be detected at the output side of the RM. The resonant angle is sensitive to the polarization of light; hence, the RM design can work in both TE and TM modes. Fig. 2a demonstrates a three-layer waveguide structure used for biosensing, in which the low RI spacer works as a resonant cavity and the high index waveguide layer acts as a reflector for incident light. If some optical absorption molecules are absorbed or bound in the evanescence field above the waveguide, the reflection of light at an appropriate wavelength will decrease. The reported detection limit of goat anti-hIgG reaches 0.5 μg/ml (approximately 3 nmol/L) (Goddard et al., 1994), and in another work from the same group, a detection limit of 19.9 fmol/mm^2 for DNA was achieved (Watts et al., 1995).

To obtain high sensitivity, it is essential to push more light into the cover layer to increase the interaction between the evanescent field and the target molecules. In this sense, a so-called reverse symmetry waveguide structure was designed (Horváth et al., 2002, 2003, 2005; Skivesen et al., 2003; Fan et al., 2008). As demonstrated in Fig. 2b, in such a configuration, the RI of the substrate is lower than that of the cover layer. In general, the material of the substrate is glass, while the spacer is nanoporous silica and the cover layer is a polymer with a high RI. Compared to RM sensors, the peak angle sensitivity of such a design is improved approximately fourfold, reaching 1.65×10^{-6} (deg/cell)/mm^2 and a detection limit of 60 cells/mm^2 for the TM mode.

As demonstrated in Fig. 2c, a metal clad leaky waveguide (MCLW) is another optical structure that involves a metal layer (Zourob et al., 2003a, 2003b; Zourob and Goddard, 2005; Skivesen et al., 2005, 2007). The motivation for this design is to increase the penetration depth; thus, it includes most of the entire volume of the samples within the evanescent field. For conventionally used waveguides such as RMs, the penetration depth is limited to several hundreds of nanometers, while the MCLW gives a penetration depth of about 1 μm into the water layer and a propagation length of a few millimeters along the waveguide. Similar to the reverse symmetry waveguide design, the larger penetration depth in the MCLW also increases the sensitivity of the system. In particular, the large penetration depth makes the detection of a large sample like bacterial spores possible. A detection limit of 8–9 cells/mm^2 has been experimentally achieved using MCLW sensors (Skivesen

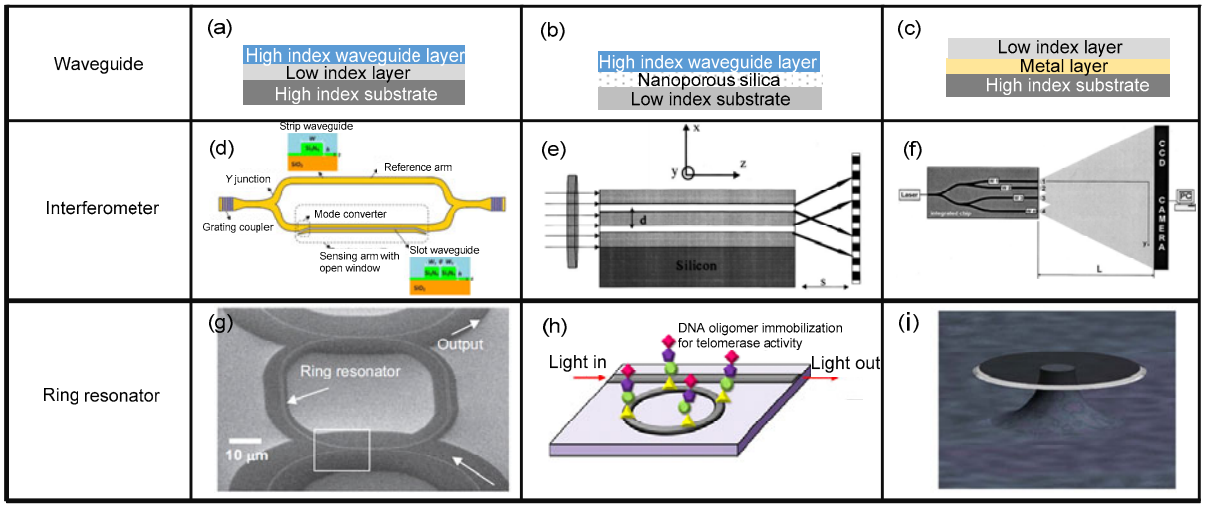

Fig. 2 Waveguide-based biosensors with different designs: (a–c) optical waveguide based biosensors; (d–f) waveguide based interferometer biosensors; (g–i) waveguide based ring resonator biosensors

(d) is reprinted from Liu Q et al. (2013), Copyright 2013, with permission from Elsevier; (e) is reprinted from Cross et al. (1999), Copyright 1999, with permission from the American Institute of Physics; (f) is reprinted from Ymeti et al. (2003), Copyright 2003, with permission from the Optical Society of America; (g) is reprinted from Taniguchi et al. (2016), Copyright 2016, with permission from Elsevier; (h) is reprinted from Kim et al. (2013), Copyright 2013, with permission from Elsevier; (i) is reprinted from Armani and Vahala (2006), Copyright 2006, with permission from the Optical Society of America

et al., 2007), and the detection of bacterial spores was also demonstrated with a detection limit of 8×10^4 spores/mL (Zourob et al., 2003a).

3.2 Waveguide based interferometer biosensors

Fig. 2d shows the schematic of a slot-waveguide-based Mach–Zehnder interferometer (MZI) biosensor. Usually, a coherent, single-frequency, single polarization laser light is coupled into the input slot waveguide through a grating coupler. Then the coupled light is split into two arms with a Y junction and recombined again after a certain distance. The reference arm consists of a strip waveguide protected by a thick cladding layer, while the sensing arm consists of a slot waveguide with a window on the top of it, allowing the evanescent field to interact with the surrounding medium. In general, the waveguide slots must maintain their polarization and be single mode to avoid interference from other modes. On the output side, the interference of light can be expressed as

$$I_{\text{out}} / I_{\text{in}} \propto 1 + V\cos(\Delta\varphi + \Delta\varphi_0), \tag{7}$$

where $\Delta\varphi=2\pi\Delta n_{\text{eff}}L/\lambda$ is the phase difference between the two arms induced by the change in the surrounding medium, $\Delta\varphi_0$ is the initial phase difference of the two arms, and L represents the length of the sensing region. From Eq. (7), we can find that increasing the length of the working region will improve the sensitivity of the biosensors. However, because the ratio $I_{\text{out}}/I_{\text{in}}$ is cosine-dependent on L, the biosensors will be insensitive near the maximum and minimum of the cosine function.

Waveguide based interferometer sensors pose strict requirements on the quality of the strip waveguides; therefore, they follow the development of the telecommunication and semiconductor industries. In 1991, an MZI biosensor with the reference arm in air was demonstrated (Heideman et al., 1991). Later, the same group demonstrated the first integrated waveguide-based MZI biosensor (Heideman et al., 1993). The authors fabricated an MZI on silicon substrate with the silica as the spacer and Si_3N_4 as the waveguide. The gratings were fabricated for input/output coupling. The detection limit of Δn was about 4×10^{-6} RIU, and the sensitivity of the system was demonstrated down to 18.9 fM in a streptavidin solution. Later, Schipper et al. (1997) designed a symmetrical MZI sensor, in which the sensor area was fabricated on two arms of the same size. Meanwhile, the authors optimized the size of the waveguide to improve the sensitivity of the sensor. The demonstrated RI change was about 1×10^{-4} RIU, and an antibody-antigen binding process was detected.

Another important improvement is the anti-resonant reflecting optical waveguide (ARROW) structure proposed by Jiménez et al. (1996). The large core dimensions on the order of micrometers make lower insertion loss possible, while the optimized waveguide structures and sizes ensure the single mode behavior and high sensitivity of the sensors. In Prieto et al. (2003), the immunoreaction a-HSA/HSA was observed with a detection limit of 1.8 ng/mm^2.

With a similar slot waveguide design, another interferometric technique based on Young's interferometer (YI) was developed for biosensing. As demonstrated in Fig. 2e, unlike the MZI which detects the output laser power recombined by the two arms, the sensing mechanism in YI is based on the detection of interference patterns formed by laser light from the two arms. The intensity distribution of interference patterns along the screen of the detector can be derived to be

$$I(y) = 1 + \cos\left(\frac{2\pi d}{\lambda D} y + \Delta\varphi\right), \tag{8}$$

where $\Delta\varphi=2\pi L/\lambda$ is the initial phase difference between the two interfering beams, d is the distance between the sensing and reference slots, D is the distance from the output side to the detecting screen, and y represents the position on the detecting screen. The phase change can also be written as $\Delta\varphi=2\pi cL\Delta n_{\text{eff}}/\lambda$, where c is the sensitivity coefficient. A change in Δn_{eff} would cause a spatial shift in interference patterns. By applying a Fourier transformation on the acquired intensity distribution, the phase value $\Delta\varphi$ can be extracted for analysis (Brandenburg and Henninger, 1994).

Brandenburg and Henninger (1994) designed an integrated YI sensor. The RI sensing of gases and fluids was demonstrated with a resolution of 1×10^{-5} RIU. Using the same design, follow-up work was done by Brandenburg (1997), improving the resolution to 1×10^{-7} RIU. Although these two works realized the integration of YI, the reference and sample

cells were fabricated in separate parts placed at the end face of the YI chip. Later, Cross et al. (1999) proposed the first dual polarization interferometry for humidity sensing. The YI sensor was based on two vertically stacked slab waveguides, and the sample cells were etched on the surface of the final layer. As a continuation of this work, the group optimized the waveguide structures and realized the detection of protein (Cross et al., 2003). The input end-face of this dual slab waveguide is uniformly illuminated with the light of a coherent source, and only the fundamental mode can maintain the propagation in the waveguides. The precision of the measurements taken was on the order of 40 pm with respect to the adsorbed adlayer thicknesses.

The MZI biosensor introduced above has achieved high sensitivity in sensing the binding and absorption of target molecules. However, the single sensing slot makes it unsuitable for multianalyte testing. As demonstrated in Fig. 2f, Ymeti et al. (2003) proposed a four-channel YI structure, enabling simultaneous and independent monitoring of three binding processes. Among the four channels, one is designated for reference while the others for sensing. The spacing between each sensing arm and the reference arm is unique, and the interference patterns can be well separated. In this work, by optimizing the design geometry and the signal processing techniques, the phase noise and inter-channel cross-talk are effectively reduced. A refractive-index resolution of 8.5×10^{-8} was achieved experimentally.

Fig. 2f demonstrates another interfering biosensor, called the Hartman interferometer (HI). A single planar wave of linearly polarized laser light is coupled into the waveguide by an input grating fabricated into the chip. Then, the broad light passes through a region with multiple parallel strips. Similar to the MZI design, integrated optical elements are used to create interference between the light from adjacent strips, which are coated with specific or nonspecific receptors. This multi-channel design not only makes multianalyte testing possible but also simplifies the fabrication and sensing process. The first biosensing demonstration with the device was done by Schneider et al. (1997), and a direct detection limit of 2 mg/L was demonstrated in sensing human chorionic gonadotropin (hCG). In follow-up work, the authors realized a one-step assay for hCG in human serum with a detection limit of 0.1 ng/mL (Schneider et al., 2000). By employing a reference sensing region to subtract the interference resulting from non-specific binding and controlling the surface chemistry of the optical chip, the non-specific adsorption signal was effectively reduced. Meanwhile, amplification of the signal was realized using gold nanoparticles.

3.3 Waveguide based ring resonator biosensors

As discussed, the sensitivity of the waveguide-based biosensors introduced above is determined by the length of the working region. However, when light is confined within a ring resonator, the effective length L_{eff} is related to the Q-factor of the resonator and defined by $L_{\mathrm{eff}}=2\pi n/\lambda$, where n is the RI of the resonator and λ is the wavelength of the detecting light (Fan et al., 2008; Flueckiger et al., 2016). Thus, by fabricating a high-Q ring resonator, the size of the biosensors can be effectively reduced, while the sensitivity of the sensors is similar or even superior to those of conventional waveguide-based sensors.

Waveguide based ring resonator biosensors are an emerging sensing technique. The working principle of this technique is based on the detection of the resonant wavelength of the system by $\lambda=2\pi n_{\mathrm{eff}}r/m$, where r is the outer radius of the ring resonator, n_{eff} is the effective index of the mode fields, and m is an integer. By detecting the shift of the resonant wavelength, the binding or absorption process between receptors and analyte molecules can be dynamically observed (Flueckiger et al., 2016).

Figs. 2g–2i demonstrate two typical waveguide-based resonators for a biosensor, i.e., ring-shaped biosensors and disk-shaped biosensors. In theory, the sensitivity of a ring resonator can reach 10^{-9} RIU (Krioukov et al., 2003; Ksendzov and Lin, 2005; Chao et al., 2006; de Vos et al., 2007; Schweinsberg et al., 2007; Fan et al., 2008; Flueckiger et al., 2016). Yet, in experiments, the surface of the ring resonator or disk is not so perfect; thus, roughness cannot be avoided. Experimental results are still a few orders of magnitude away from this standard. A biosensor of a vertically coupled glass microring resonator with a Q-factor of about 12 000 was proposed by Krioukov et al. (2003), and the RI sensitivity was calculated to be 1.8×10^{-5} RIU. In Yalcin et al. (2016), polymer microring resonators were demonstrated for biosensing

with a Q-factor of about 20 000, and a detection limit of 10^{-7} RIU was achieved.

Meanwhile, ring resonators with subwavelength gratings (Flueckiger et al., 2016) and a trapping-assisted microdonut (Lin SY and Crozier, 2013) were proposed. The ring resonator with subwavelength gratings worked in the TE mode, and was two times as sensitive as the best TM ring and slot resonators. The reported sensitivity was about 400–500 nm/RIU (Flueckiger et al., 2016). The Q-factor of the trapping-assisted microdonut was about 9000 with a sensitivity of 2.1±0.4 pm. The optical trapping assisted sensing technique has the advantage of reusability, and enables the detection of different molecules (Lin SY and Crozier, 2013).

4 Chip-based waveguide micro/nanoscopy

4.1 Fluorescence labeling chip based micro/nanoscopy

In Agnarsson et al. (2009), an evanescent-wave fluorescence excitation method based on symmetric planar waveguides was proposed (Fig. 3a). The light was coupled through a single-mode optical fiber into the planar waveguide. Using waveguides with a symmetric cladding environment, in-coupling of the excitation light was greatly simplified and intensity uniformity of the evanescence illumination improved. Later, a light-emitting diode (LED) based waveguide TIRF system was designed (Hassanzadeh et al., 2008). High-power LEDs functioned as the light source. A coverslip waveguide was used to provide a wide-field uniform evanescence illumination (Fig. 3b). No alignment was required for this system and high contrast in vivo biological imaging achieved. Though these techniques acquired high-quality images of fluorescence labeled cells or tissues over large fields of view (FOVs), none of them realized imaging with a resolution beyond the diffraction limit.

Recently, chip-based single molecule localization microscopy (chip-based dSTORM) was reported (Diekmann et al., 2017). Although it is the same as the STORM technique, only a fraction of the fluorophores were turned on in each imaging cycle. After a series of imaging cycles, the overall image was reconstructed with nanometer accuracy. As demonstrated in Figs. 3c and 3d, channel-like waveguides with a tantalum pentoxide (Ta_2O_5) rib or strip geometry were fabricated to provide evanescent field illumination. A resolution better than 50 nm was demonstrated in imaging immunostained microtubules in rat liver sinusoidal endothelial cells (LSECs) and DNA-origami nanorulers. For this chip-based

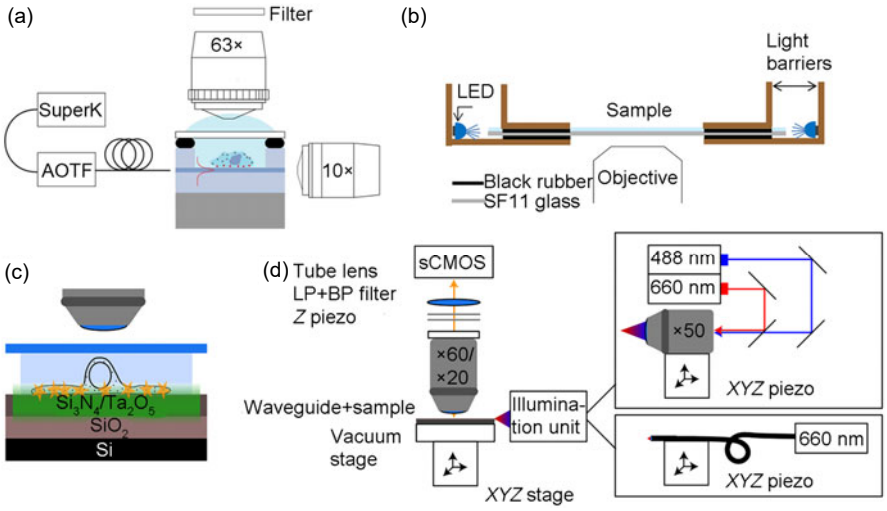

Fig. 3 Schematic illustration of the experimental configuration for an evanescent-wave fluorescence excitation method based on symmetric planar waveguides (a), schematic of the LED-based waveguide TIRF microscopy system (b), implementation of chip-based nanoscopy where light guided inside the waveguide is the source of the evanescent field illuminating samples on top of the surface (c), and the optical setup for the whole imaging system (d)

(a) is reprinted from Agnarsson et al. (2009), Copyright 2009, with permission from the Optical Society of America; (b) is reprinted from Ramachandran et al. (2013), Copyright 2013, with permission from Springer Nature; (c) and (d) are reprinted from Diekmann et al. (2017), Copyright 2017, with permission from Springer Nature

dSTORM technique, the FOV of the system was about several hundred micrometers square under a 60× 1.2NA objective lens (Fig. 3d). The time required for acquiring all raw images was around 0.5 h (about 30000 frames and 50 ms exposure time for each frame).

Using the same setup, chip-based entropy-based super-resolution imaging (ESI) was demonstrated as well. The ESI imaging technique is based on reconstructing super-resolved images from image sequences with rapid random signal fluctuations, which can work with dynamic events like on-off switching of the fluorescent dyes and photobleaching (Yahiatène et al., 2015). By calculating the local entropy (H) and cross-entropy (xH) values pixel by pixel, a super-resolved image of the sample can be reconstructed. Compared to the dSTORM acquisition procedure where single molecule switching is required, the input power is lower for chip-based ESI. Meanwhile, there is no need to further control the illumination pattern. Pictures of about 200 frames were recorded for ESI reconstruction, and a resolution of 106 nm was achieved in the ESI image.

Fluorescence labeled chip based waveguide microscopy combines the advantages of conventional fluorescent microscopy and dark field imaging, achieving a high signal-to-noise ratio (SNR) image in a wide FOV with tens of nanometers resolution. The complexity of the entire optical setup is highly reduced by removing the excitation light path.

4.2 Label-free chip based waveguide micro/nanoscopy

To complement the chip-based waveguide super-resolution imaging based on fluorescence, various label-free chip based waveguide super-resolution imaging techniques were developed. Hao et al. (2013) proposed a super-resolution imaging technique, which uses the evanescence field around a micro optical fiber as the light source. In this work, the resolution of the system was improved from 457 to about 300 nm. However, the FOV of this technique was confined to within a small area around the fiber, and it could realize only one-dimensional (1D) super-resolution imaging unless moving the fiber probe or the sample stage in the circular scanning method. In addition, the resolution of this technique is limited by the RI of silica, and its SNR is poor. Later, Agnarsson et al. (2015) developed a label-free super-resolution waveguide chip, consisting of a 400-nm thick silica core embedded in a symmetric 4-μm thick CYTOP cladding layer. In this work, the design realized the observation of 150 nm fluorescently labeled vesicles in both fluorescence and scattering modes. Compared to the fiber probe, the FOV of this design achieved a high improvement. However, as demonstrated in Fig. 4a, useful subwavelength information can be recovered only along the illumination direction, and the unidirectional illumination in this design cannot resolve complex two-dimensional (2D) samples as well.

One-dimensional light emitters have shown strong light localization, an ultrasmall footprint, perfect mechanical flexibility, and high fluorescent efficiency, thus showing great potential in micro/nanoscopy (Tong et al., 2003; Ma et al., 2003; Tian et al., 2010; Yang et al., 2011). Using a nanowire ring as the light source, Liu XW et al. (2017) designed a new chip-based waveguide super-resolution technique, called NWR illumination microscopy (NWRIM) (Fig. 4b). In this work, a silicon wafer cutting coated with a 200-nm aluminum oxide (Al_2O_3) or titanium dioxide (TiO_2) film worked as the substrate to support the samples and nanowire light emitters. When the semiconductor nanowire ring was excited by an external laser, the fluorescence emitted from the nanowires coupled into the film waveguide and propagated towards the samples. Compared to previous label-free chip based waveguide super-resolution techniques, NWRIM achieved a higher resolution (about 140 nm). The 360° evanescence illumination also guarantees the resolution of simple 2D subwavelength structures. The reported FOV in this work was about 1000 μm^2, which is one order of magnitude greater than previous results.

Later, by optimizing the deposition conditions, film waveguides with higher refractive indices and better surface quality were fabricated. High contrast-to-noise ratio (CNR) sub-diffraction imaging with lateral resolution of 122 nm was experimentally achieved (Figs. 4c and 4d) (Pang et al., 2017). In this work, the FOV of the system achieved a further six-fold increase to 6000 μm^2. Meanwhile, the authors demonstrated a polarization selectivity in the imaging process (Figs. 4e and 4f). By adding a rotatable polarizer in front of the detector, the CNR of the system acquired another four-fold improvement.

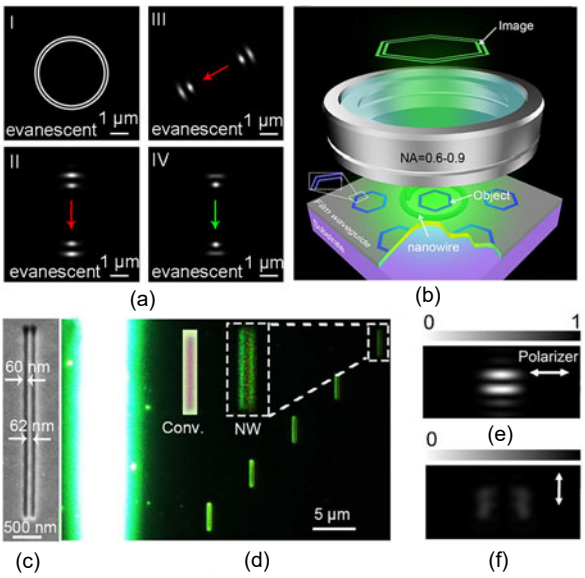

Fig. 4 Simulated images of sub-wavelength structures under unidirectional evanescent field illumination: (a) simulated pattern comprising two concentric rings where the center-to-center distance is 160 nm and the linewidth is 80 nm (I) and the corresponding images for different evanescent wave illuminations along the arrow (II–IV); (b) schematic of the NWRIM configuration and imaging process (under an omnidirectional evanescent illumination from the fluorescent NWR, the sub-diffraction nested features of the central hexagon show up in the far-field image); (c) SEM images of the groove pairs when titanium dioxide layers are deposited at 300 °C where the depth of the groove pair is 76 nm; (d) the corresponding optical images of the groove pairs under evanescent field illumination; (e, f) simulation results for the far-field images of the groove pair under S and P wave illumination, respectively

(a) is reprinted from Pang et al. (2019), Copyright 2019, with permission from the authors; (b) is reprinted from Liu XW et al. (2017), Copyright 2017, with permission from the American Physical Society; (c)–(f) are reprinted from Pang et al. (2017), Copyright 2017, with permission from the Optical Society of America

By shifting the high spatial frequency information of subwavelength samples to the passband of a microscope system, techniques based on a frequency-shift effect have demonstrated optical super-resolution capability. However, under evanescence illumination with a given wave vector $k_{\text{eva.}}=2\pi n_{\text{eff}}/\lambda_{\text{eva.}}$ ($\lambda_{\text{eva.}}$ is the wavelength of the evanescence field), only the spatial frequency information around ($-k_{\text{eva.}}\cos\theta$, $-k_{\text{eva.}}\sin\theta$) with a radius of $k_{\text{ceva.}}=2\pi\text{NA}/\lambda_{\text{eva.}}$ is collectable. Thus, the NWRIM technique is unable to resolve complex 2D structures, as the sizes of the illumination wave vectors are identical. Meanwhile, because of frequency aliasing, it is impossible for the NWRIM technique to recover the real size of the samples.

Recently, Pang et al. (2019) proposed a novel super-resolution chip (SRC), which realized the illumination of a sample with multi-color evanescent waves traveling along different directions. In this work, a wide-band polymer fluorescent film was used to illuminate the sample paced within a polygon working region (Fig. 5a). By locally exciting different edges of the polygonal fluorescent polymer films, high-frequency components along the given directions were acquired separately, enabling recovery of high-frequency information for the samples. The time consumption to acquire one image under a given wave vector was about 10 s. To reconstruct a 2D sample, the direction numbers needed for evanescence illumination and oblique illumination were about 20 and 6, respectively, and the time consumption was about 8 min. By frequency shifting and iterative stitching of different spatial frequencies in the Fourier space, a wide spatial frequency spectrum of the 2D sample was achieved (Fig. 5b). The authors demonstrated the capability of such an SRC by imaging different 2D samples like the Chinese character for "light" (Fig. 5c) and carbon nanotubes (Fig. 5e). The final reconstructed image matched well with scanning electron microscopy (SEM) and atomic force microscopy (AFM) images in telling the real size of the sample (Figs. 5d–5f).

5 Conclusions and perspective

In this review paper, we summarized some chip-based waveguide sensing and imaging techniques. On one hand, using the evanescence field generated around the waveguide surface to interact with molecules located within it, the binding and absorption processes could be observed. On the other hand, the generated evanescence field could interact with the sample directly and shift the high spatial frequency information of the samples into the microscope system's passband. The eventual goal of both waveguide-based biosensors and super-resolution imaging chips is to develop portable devices.

Waveguide-based biosensors have been under development for several decades, and some of them have been commercialized. With the development of smartphones, the concept of mobile health has been proposed and related smartphone-based biosensors have been reported (Yu et al., 2015; Zhang JL et al., 2018; Guner et al., 2019). In general, the smartphone-based biosensors can be divided into two categories, i.e., the smartphone as detector and the smartphone as instrumentation interface. For the former, the smartphone works as a detector. An apparatus which combines a disposable substrate, the illumination light source, and related optical elements is integrated with the phone via a 3D printed holder (Figs. 6a and 6b). An alternative approach has the smartphone connected with the experimental setup via a micro-USB port, Bluetooth, or Wi-Fi (Figs. 6c–6e). The smartphone works for only displaying the testing results and controlling the experimental setup. For details, please refer to Roda et al. (2016). In the future, a portable multifunctional biosensor, similar to the Apple Watch, will achieve many applications in healthcare.

The chip-based waveguide implementation has dramatically reduced the complexity of the imaging system, and the fluorescent labeling chip based super-resolution imaging techniques have great potential for a wider range of use. The waveguide-based dSTORM

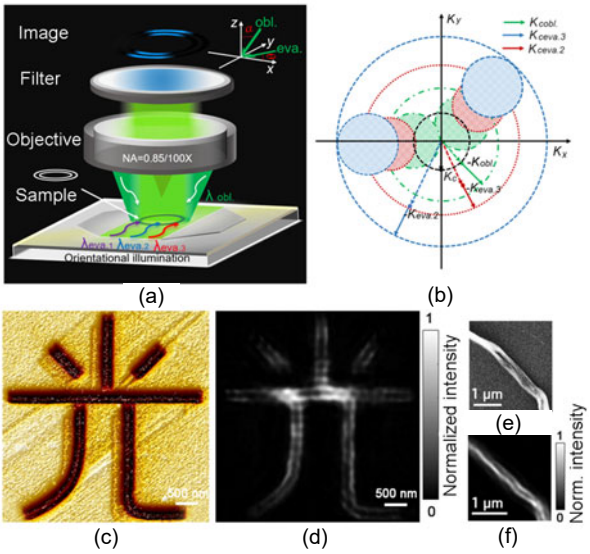

Fig. 5 Schematic of the evanescent field illumination and oblique illumination process (a), schematic of the reconstruction method (b), AFM image of the etched Chinese character for "light" (c), reconstructed image of the Chinese character for "light" (d), SEM image of a carbon nanotube sample (e), and reconstructed image of the carbon nanotube sample (f)

Reprinted from Pang et al. (2019), Copyright 2019, with permission from the authors. In (a), under a given illumination direction, the object (here a circular ring pair) is partially resolved at different wavelengths using the appropriate bandpass filters. In the diagram, θ represents the illumination direction and α is the angle of incidence for oblique illumination (obl. means oblique illumination; eva. represents evanescent illumination). In (b), K_c, $K_{cobl.}$, $K_{ceva.2}$, and $K_{ceva.3}$ are the cut-off wavenumbers of the microscope system for different illumination modes and wavelengths, $K_{obl.}$ is the wave vector under oblique illumination, and $K_{eva.2}$ and $K_{eva.3}$ are the wave vectors for evanescent field illumination at wavelengths of λ_2 and λ_3, respectively

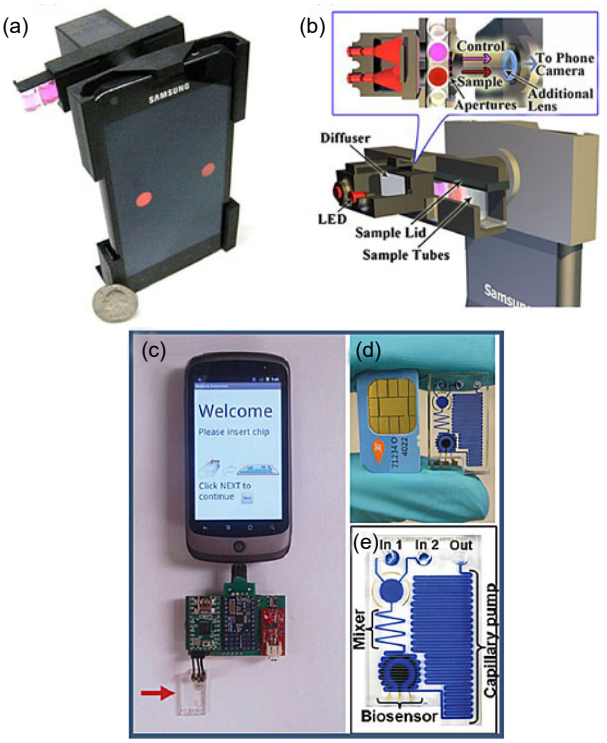

Fig. 6 Image of the iTube platform and smartphone screen for the colorimetric assay reading (a), a schematic illustration of the components of the same iTube platform (b), photograph of the assembled prototype device in which the arrow indicates the microfluidic chip (c), photograph of the chip and a cellphone SIM card for comparison (d), and an enlarged image of the chip with labeled components in which the channels are filled with dye for improved visualization of the fluidic network (e)

(a) and (b) are reprinted from Coskun et al. (2013), Copyright 2013, with permission from the Royal Society of Chemistry; (c)–(e) are reprinted from Lillehoj et al. (2013), Copyright 2013, with permission from the Royal Society of Chemistry

introduced has realized tens of nanometers resolution, but the whole imaging process is still time-consuming (about 30 min). The development of more sensitive detectors/cameras will further speed up image acquisition. Meanwhile, the coupling of light into the waveguide through optical fibers or an objective lens is still complex for practical use. With the developments in photonic integrated circuits (PIC), future on-chip laser sources will make the system more compact and easier to use. On the other hand, with the development of micro/nano fabrication techniques, a polygon planar waveguide with multiple incident ports could be fabricated. By designing the corresponding coupling structures connected to each port, the laser light at different wavelengths would couple into the waveguide to interact with the sample placed on the surface of the working region. The development of chip-based light sources also provides the possibility to realize self-powered label-free waveguide based super-resolution imaging.

Contributors

Chen-lei PANG designed the research and drafted the manuscript. Qing YANG helped organize the manuscript. Xu LIU and Wei CHEN revised the manuscript. Chen-lei PANG and Qing YANG finalized the paper.

Compliance with ethics guidelines

Chen-lei PANG, Xu LIU, Wei CHEN, and Qing YANG declare that they have no conflict of interest.

References

Abbe E, 1873. Beiträge zur theorie des mikroskops und der mikroskopischen wahrnehmung. *Arch f Mikrosk Anat*, 9(1):413-418 (in German). https://doi.org/10.1007/BF02956173

Agnarsson B, Ingthorsson S, Gudjonsson T, et al., 2009. Evanescent-wave fluorescence microscopy using symmetric planar waveguides. *Opt Expr*, 17(7):5075-5082. https://doi.org/10.1364/OE.17.005075

Agnarsson B, Lundgren A, Gunnarsson A, et al., 2015. Evanescent light-scattering microscopy for label-free interfacial imaging: from single sub-100 nm vesicles to live cells. *ACS Nano*, 9(12):11849-11862. https://doi.org/10.1021/acsnano.5b04168

Armani AM, Vahala KJ, 2006. Heavy water detection using ultra-high-Q microcavities. *Opt Lett*, 31(23):1896-1898. https://doi.org/10.1364/OL.31.001896

Axelrod D, 2001. Total internal reflection fluorescence microscopy in cell biology. *Traffic*, 2(11):764-774. https://doi.org/10.1034/j.1600-0854.2001.21104.x

Axelrod D, Thompson NL, Burghardt TP, 1983. Total internal reflection fluorescent microscopy. *J Microsc-Oxford*, 129(1):19-28. https://doi.org/10.1111/j.1365-2818.1983.tb04158.x

Bates M, Huang B, Dempsey GT, et al., 2007. Multicolor super-resolution imaging with photo-switchable fluorescent probes. *Science*, 317(5845):1749-1753. https://doi.org/10.1126/science.1146598

Betzig E, Trautman JK, 1992. Near-field optics: microscopy, spectroscopy, and surface modification beyond the diffraction limit. *Science*, 257(5067):189-195. https://doi.org/10.1126/science.257.5067.189

Betzig E, Patterson GH, Sougrat R, et al., 2006. Imaging intracellular fluorescent proteins at nanometer resolution. *Science*, 313(5793):1642-1645. https://doi.org/10.1126/science.1127344

Brandenburg A, 1997. Differential refractometry by an integrated-optical Young interferometer. *Sens Actuat B Chem*, 39(1-3):266-271. https://doi.org/10.1016/S0925-4005(97)80216-X

Brandenburg A, Henninger R, 1994. Integrated optical Young interferometer. *Appl Opt*, 33(25):5941-5947. https://doi.org/10.1364/AO.33.005941

Chao CY, Fung W, Guo LJ, 2006. Polymer microring resonators for biochemical sensing applications. *IEEE J Sel Top Quant*, 12(1):134-142. https://doi.org/10.1109/JSTQE.2005.862945

Chung JW, Bernhardt R, Pyun JC, 2006. Additive assay of cancer marker CA 19-9 by SPR biosensor. *Sens Actuat B Chem*, 118(1-2):28-32. https://doi.org/10.1016/j.snb.2006.04.015

Coskun AF, Wong J, Khodadadi D, et al., 2013. A personalized food allergen testing platform on a cellphone. *Lab Chip*, 13(4):636-640. https://doi.org/10.1039/C2LC41152K

Cross GH, Ren YT, Freeman NJ, 1999. Young's fringes from vertically integrated slab waveguides: applications to humidity sensing. *J Appl Phys*, 86(11):6483-6488. https://doi.org/10.1063/1.371712

Cross GH, Reeves AA, Brand S, et al., 2003. A new quantitative optical biosensor for protein characterisation. *Biosens Bioelectron*, 19(4):383-390. https://doi.org/10.1016/S0956-5663(03)00203-3

Cush R, Cronin JM, Stewart WJ, et al., 1993. The resonant mirror: a novel optical biosensor for direct sensing of biomolecular interactions. Part I: principle of operation and associated instrumentation. *Biosens Bioelectron*, 8(7-8):347-354. https://doi.org/10.1016/0956-5663(93)80073-X

Darafsheh A, Walsh GF, Dal Negro L, et al., 2012. Optical super-resolution by high-index liquid-immersed microspheres. *Appl Phys Lett*, 101(14):141128. https://doi.org/10.1063/1.4757600

de Vos K, Bartolozzi I, Schacht E, et al., 2007. Silicon-on-insulator microring resonator for sensitive and label-free biosensing. *Opt Expr*, 15(12):7610-7615. https://doi.org/10.1364/OE.15.007610

Diekmann R, Helle ØI, Øie CI, et al., 2017. Chip-based wide field-of-view nanoscopy. *Nat Photon*, 11(5):322-328. https://doi.org/10.1038/nphoton.2017.55

Fan XD, White IM, Shopova S, et al., 2008. Sensitive optical biosensors for unlabeled targets: a review. *Anal Chim Acta*, 620(1-2):8-26. https://doi.org/10.1016/j.aca.2008.05.022

Flueckiger J, Schmidt S, Donzella V, et al., 2016. Sub-wavelength grating for enhanced ring resonator biosensor. *Opt Expr*, 24(14):15672-15686. https://doi.org/10.1364/OE.24.015672

Goddard NJ, Pollard-Knight D, Maule CH, 1994. Real-time biomolecular interaction analysis using the resonant mirror sensor. *Analyst*, 119(4):583-588. https://doi.org/10.1039/AN9941900583

Goddard NJ, Singh K, Hulme JP, et al., 2002. Internally-referenced resonant mirror devices for dispersion compensation in chemical sensing and biosensing applications. *Sens Actuat A*, 100(1):1-9. https://doi.org/10.1016/S0924-4247(02)00062-6

Graham CR, Leslie D, Squirrell DJ, 1992. Gene probe assays on a fibre-optic evanescent wave biosensor. *Biosens Bioelectron*, 7(7):487-493. https://doi.org/10.1016/0956-5663(92)80005-V

Grandin HM, Städler B, Textor M, et al., 2006. Waveguide excitation fluorescence microscopy: a new tool for sensing and imaging the biointerface. *Biosens Bioelectron*, 21(8):1476-1482. https://doi.org/10.1016/j.bios.2005.06.011

Guner H, Ozgur E, Kokturk G, et al., 2019. A smartphone based surface plasmon resonance imaging (SPRi) platform for on-site biodetection. *Sens Actuat B Chem*, 239:571-577. https://doi.org/10.1016/j.snb.2016.08.061

Gustafsson MGL, 2005. Nonlinear structured-illumination microscopy: wide-field fluorescence imaging with theoretically unlimited resolution. *Proc Natl Acad Sci USA*, 102(37):13081-13086. https://doi.org/10.1073/pnas.0406877102

Gustafsson MGL, Shao L, Carlton PM, et al., 2008. Three-dimensional resolution doubling in wide-field fluorescence microscopy by structured illumination. *Biophys J*, 94(12):4957-4970. https://doi.org/10.1529/biophysj.107.120345

Hanumegowda NM, White IM, Oveys H, et al., 2005. Label-free protease sensors based on optical microsphere resonators. *Sens Lett*, 3(4):315-319. https://doi.org/10.1166/sl.2005.044

Hao X, Kuang CF, Liu X, et al., 2011. Microsphere based microscope with optical super-resolution capability. *Appl Phys Lett*, 99(20):203102. https://doi.org/10.1063/1.3662010

Hao X, Liu X, Kuang CF, et al., 2013. Far-field super-resolution imaging using near-field illumination by micro-fiber. *Appl Phys Lett*, 102(1):013104. https://doi.org/10.1063/1.4773572

Hassanzadeh A, Nitsche M, Mittler S, et al., 2008. Waveguide evanescent field fluorescence microscopy: thin film fluorescence intensities and its application in cell biology. *Appl Phys Lett*, 92(23):233503. https://doi.org/10.1063/1.2937840

Hastings JT, Guo J, Keathley PD, et al., 2007. Optimal self-referenced sensing using long- and short-range surface plasmons. *Opt Expr*, 15(26):17661-17672. https://doi.org/10.1364/OE.15.017661

Hecht B, Sick B, Wild UP, et al., 2000. Scanning near-field optical microscopy with aperture probes: fundamentals and applications. *J Chem Phys*, 12(18):7761-7774. https://doi.org/10.1063/1.481382

Heideman RG, Kooyman RPH, Greve J, et al., 1991. Simple interferometer for evanescent field refractive index sensing as a feasibility study for an immunosensor. *Appl Opt*, 30(12):1474-1479. https://doi.org/10.1364/AO.30.001474

Heideman RG, Kooyman RPH, Greve J, 1993. Performance of a highly sensitive optical waveguide Mach–Zehnder interferometer immunosensor. *Sens Actuat B Chem*, 10(3): 209-217. https://doi.org/10.1016/0925-4005(93)87008-D

Hess ST, Girirajan TPK, Mason MD, 2006. Ultra-high resolution imaging by fluorescence photoactivation localization microscopy. *Biophys J*, 91(11):4258-4272. https://doi.org/10.1529/biophysj.106.091116

Hoa XD, Kirk AG, Tabrizian M, 2007. Towards integrated and sensitive surface plasmon resonance biosensors: a review of recent progress. *Biosens Bioelectron*, 23(2):151-160. https://doi.org/10.1016/j.bios.2007.07.001

Homola J, Yee SS, Gauglitz G, 1999. Surface plasmon resonance sensors. *Sens Actuat B Chem*, 54(1-2):3-15. https://doi.org/10.1016/S0925-4005(98)00321-9

Horváth R, Lindvold LR, Larsen NB, 2002. Reverse-symmetry waveguides: theory and fabrication. *Appl Phys B*, 74(4-5):383-393. https://doi.org/10.1007/s003400200823

Horváth R, Pedersen HC, Skivesen N, et al., 2003. Optical waveguide sensor for on-line monitoring of bacteria. *Opt Lett*, 28(14):1233-1235. https://doi.org/10.1364/OL.28.001233

Horváth R, Pedersen HC, Skivesen N, et al., 2005. Monitoring of living cell attachment and spreading using reverse symmetry waveguide sensing. *Appl Phys Lett*, 86(7): 071101. https://doi.org/10.1063/1.1862756

Jiménez D, Bartolomé E, Moreno M, et al., 1996. An integrated silicon ARROW Mach–Zehnder interferometer for sensing applications. *Opt Commun*, 132(5-6):437-441. https://doi.org/10.1016/0030-4018(96)00387-2

Kim J, Song KB, 2007. Recent progress of nano-technology with NSOM. *Micron*, 38(4):409-426. https://doi.org/10.1016/j.micron.2006.06.010

Kim J, Shin Y, Perera AP, et al., 2013. Label-free, PCR-free chip-based detection of telomerase activity in bladder cancer cells. *Biosens Bioelectron*, 45:152-157. https://doi.org/10.1016/j.bios.2013.02.001

Klar TA, Engel E, Hell SW, 2001. Breaking Abbe's diffraction

resolution limit in fluorescence microscopy with stimulated emission depletion beams of various shapes. *Phys Rev E Stat Nonl Soft Matter Phys*, 64(6):066613. https://doi.org/10.1103/PhysRevE.64.066613

Krioukov E, Greve J, Otto C, 2003. Performance of integrated optical microcavities for refractive index and fluorescence sensing. *Sens Actuat B Chem*, 90(1-3):58-67. https://doi.org/10.1016/S0925-4005(03)00022-4

Ksendzov A, Lin Y, 2005. Integrated optics ring-resonator sensors for protein detection. *Opt Lett*, 30(24):3344-3346. https://doi.org/10.1364/OL.30.003344

Lee D, Kim YD, Kim M, et al., 2017. Realization of wafer-scale hyperlens device for sub-diffractional biomolecular imaging. *ACS Photon*, 5(7):2549-2554. https://doi.org/10.1021/acsphotonics.7b01182

Liedberg B, Nylander C, Lunström I, 1983. Surface plasmon resonance for gas detection and biosensing. *Sens Actuat*, 4(2):299-304. https://doi.org/10.1016/0250-6874(83)85036-7

Lillehoj PB, Huang MC, Truong N, et al., 2013. Rapid electrochemical detection on a mobile phone. *Lab Chip*, 13(15):2950-2955. https://doi.org/10.1039/C3LC50306B

Lin SY, Crozier KB, 2013. Trapping-assisted sensing of particles and proteins using on-chip optical microcavities. *ACS Nano*, 7(2):1720-1730. https://doi.org/10.1021/nn305826j

Lin VSY, Motesharei K, Dancil KPS, et al., 1997. A porous silicon-based optical interferometric biosensor. *Science*, 278(5339):840-843. https://doi.org/10.1126/science.278.5339.840

Liu Q, Tu XG, Woo KK, et al., 2013. Highly sensitive Mach–Zehnder interferometer biosensor based on silicon nitride slot waveguide. *Sens Actuat B Chem*, 188:681-688. https://doi.org/10.1016/j.snb.2013.07.053

Liu XW, Kuang CF, Hao X, et al., 2017. Fluorescent nanowire ring illumination for wide-field far-field subdiffraction imaging. *Phys Rev Lett*, 118(7):076101. https://doi.org/10.1103/PhysRevLett.118.076101

Liu ZW, Lee H, Xiong Y, et al., 2007. Far-field optical hyperlens magnifying sub-diffraction-limited objects. *Science*, 315(5819):1686. https://doi.org/10.1126/science.1137368

Ma DDD, Lee CS, Au FCK, et al., 2003. Small-diameter silicon nanowire surfaces. *Science*, 299(5614):1874-1877. https://doi.org/10.1126/science.1080313

Millan KM, Saraullo A, Mikkelsen SR, 1994. Voltammetric DNA biosensor for cystic fibrosis based on a modified carbon paste electrode. *Anal Chem*, 66(18):2943-2948. https://doi.org/10.1021/ac00090a023

Moerner WE, 2007. New directions in single-molecule imaging and analysis. *Proc Natl Acad Sci USA*, 104(31):12596-12602. https://doi.org/10.1073/pnas.0610081104

Nikitin PI, Grigorenko AN, Beloglazov AA, et al., 2000. Surface plasmon resonance interferometry for microarray biosensing. *Sens Actuat A*, 85(1-3):189-193. https://doi.org/10.1016/S0924-4247(00)00386-1

Noto M, Khoshsima M, Keng D, et al., 2005. Molecular weight dependence of a whispering gallery mode biosensor. *Appl Phys Lett*, 87(22):223901. https://doi.org/10.1063/1.2137902

Pang CL, Liu XW, Zhuge MH, et al., 2017. High-contrast wide-field evanescent wave illuminated subdiffraction imaging. *Opt Lett*, 42(21):4569-4572. https://doi.org/10.1364/OL.42.004569

Pang CL, Li JX, Tang MW, et al., 2019. On-chip super-resolution imaging with fluorescent polymer films. *Adv Funct Mat*, 29(27):1900126. https://doi.org/10.1002/adfm.201900126

Prakash PA, Yogeswaran U, Chen SM, 2009. A review on direct electrochemistry of catalase for electrochemical sensors. *Sensors*, 9(3):1821-1844. https://doi.org/10.3390/s90301821

Prieto F, Sepúlveda B, Calle A, et al., 2003. Integrated Mach–Zehnder interferometer based on ARROW structures for biosensor applications. *Sens Actuat B Chem*, 92(1-2):151-158. https://doi.org/10.1016/S0925-4005(03)00257-0

Ramachandran S, Cohen DA, Quist AP, et al., 2013. High performance, LED powered, waveguide based total internal reflection microscopy. *Sci Rep*, 3:2133. https://doi.org/10.1038/srep02133

Rho J, Ye ZL, Xiong Y, et al., 2010. Spherical hyperlens for two-dimensional sub-diffractional imaging at visible frequencies. *Nat Commun*, 1:143. https://doi.org/10.1038/ncomms1148

Roda A, Michelini E, Zangheri M, et al., 2016. Smartphone-based biosensors: a critical review and perspectives. *Trends Anal Chem*, 79:317-325. https://doi.org/10.1016/j.trac.2015.10.019

Rotenberg N, Kuipers L, 2014. Mapping nanoscale light fields. *Nat Photon*, 8(12):919-926. https://doi.org/10.1038/nphoton.2014.285

Schermelleh L, Heintzmann R, Leonhardt H, 2010. A guide to super-resolution fluorescence microscopy. *J Cell Biol*, 190(2):165-175. https://doi.org/10.1083/jcb.201002018

Schipper EF, Brugman AM, Dominguez C, et al., 1997. The realization of an integrated Mach–Zehnder waveguide immunosensor in silicon technology. *Sens Actuat B Chem*, 40(2-3):147-153. https://doi.org/10.1016/S0925-4005(97)80254-7

Schneider BH, Edwards JG, Hartman NF, 1997. Hartman interferometer: versatile integrated optic sensor for label-free, real-time quantification of nucleic acids, proteins, and pathogens. *Clin Chem*, 43(9):1757-1763.

Schneider BH, Dickinson EL, Vach MD, et al., 2000. Highly sensitive optical chip immunoassays in human serum. *Biosens Bioelectron*, 15(1-2):13-22. https://doi.org/10.1016/S0956-5663(00)00056-7

Schweinsberg A, Hocdé S, Lepeshkin N, et al., 2007. An environmental sensor based on an integrated optical whispering gallery mode disk resonator. *Sens Actuat B*

Chem, 123(2):727-732. https://doi.org/10.1016/j.snb.2006.10.007

Serpengüzel A, Arnold S, Griffel G, 1995. Excitation of resonances of microspheres on an optical fiber. *Opt Lett*, 20(7):654-656. https://doi.org/10.1364/OL.20.000654

Skivesen N, Horvath R, Pedersen HC, 2003. Multimode reverse-symmetry waveguide sensor for broad-range refractometry. *Opt Lett*, 28(24):2473-2475. https://doi.org/10.1364/OL.28.002473

Skivesen N, Horvath R, Pedersen HC, 2005. Optimization of metal-clad waveguide sensors. *Sens Actuat B Chem*, 106(2):668-676. https://doi.org/10.1016/j.snb.2004.09.014

Skivesen N, Horvath R, Thinggaard S, et al., 2007. Deep-probe metal-clad waveguide biosensors. *Biosens Bioelectron*, 22(7):1282-1288. https://doi.org/10.1016/j.bios.2006.05.025

Su H, Kallury KMR, Thompson M, et al., 1994. Interfacial nucleic acid hybridization studied by random primer 32P labeling and liquid-phase acoustic network analysis. *Anal Chem*, 66(6):769-777. https://doi.org/10.1021/ac00078a002

Sun JB, Shalaev MI, Litchinitser NM, 2015. Experimental demonstration of a non-resonant hyperlens in the visible spectral range. *Nat Commun*, 6:7201. https://doi.org/10.1038/ncomms8201

Sundram V, Nanda JS, Rajagopal K, et al., 1993. Domain truncation studies reveal that the streptokinase-plasmin activator complex utilizes long range protein-protein interactions with macromolecular substrate to maximize catalytic turnover. *J Biol Chem*, 278(33):30569-30577. https://doi.org/10.1074/jbc.M303799200

Suter JD, White IM, Zhu HY, et al., 2007. Thermal characterization of liquid core optical ring resonator sensors. *Appl Opt*, 46(3):386-389. https://doi.org/10.1364/AO.46.000389

Taniguchi T, Hirowatari A, Ikeda T, et al., 2016. Detection of antibody-antigen reaction by silicon nitride slot-ring biosensors using protein G. *Opt Commun*, 365:16-23. https://doi.org/10.1016/j.optcom.2015.11.068

Teraoka I, Arnold S, 2006. Theory of resonance shifts in TE and TM whispering gallery modes by nonradial perturbations for sensing applications. *J Opt Soc Am B*, 23(7):1381-1389. https://doi.org/10.1364/JOSAB.23.001381

Tian BZ, Cohen-Karni T, Qing Q, et al., 2010. Three-dimensional, flexible nanoscale field-effect transistors as localized bioprobes. *Science*, 329(5993):830-834. https://doi.org/10.1126/science.1192033

Tiefenthaler K, Lukosz W, 1989. Sensitivity of grating couplers as integrated-optical chemical sensors. *J Opt Soc Am B*, 6(2):209-220. https://doi.org/10.1364/JOSAB.6.000209

Tong L, Gattass RR, Ashcom JB, et al., 2003. Subwavelength-diameter silica wires for low-loss optical wave guiding. *Nature*, 426(6968):816-819. https://doi.org/10.1038/nature02193

Wang ZB, Guo W, Li L, et al., 2011. Optical virtual imaging at 50 nm lateral resolution with a white-light nanoscope. *Nat Commun*, 2:218. https://doi.org/10.1038/ncomms1211

Watts HJ, Lowe CR, Pollard-Knight DV, 1994. Optical biosensor for monitoring microbial cells. *Anal Chem*, 66(15):2465-2470. https://doi.org/10.1021/ac00087a010

Watts HJ, Yeung D, Partees H, 1995. Real-time detection and quantification of DNA hybridization by an optical biosensor. *Anal Chem*, 67(23):4283-4289. https://doi.org/10.1021/ac00119a013

Weisser M, Tovar G, Mittler-Neher S, et al., 1999. Specific bio-recognition reactions observed with an integrated Mach–Zehnder interferometer. *Biosens Bioelectron*, 14(4):405-411. https://doi.org/10.1016/S0956-5663(98)00124-9

White IM, Fan XD, 2008. On the performance quantification of resonant refractive index sensors. *Opt Expr*, 16(2):1020-1028. https://doi.org/10.1364/OE.16.001020

White IM, Gohring J, Fan XD, 2007. SERS-based detection in an optofluidic ring resonator platform. *Opt Expr*, 15(25):17433-17442. https://doi.org/10.1364/OE.15.017433

Willig KI, Rizzoli SO, Westphal V, et al., 2006. STED microscopy reveals that synaptotagmin remains clustered after synaptic vesicle exocytosis. *Nature*, 440(7086):935-939. https://doi.org/10.1038/nature04592

Yahiatène I, Hennig S, Müller M, et al., 2015. Entropy-based super-resolution imaging (ESI): from disorder to fine detail. *ACS Photon*, 2(8):1049-1056. https://doi.org/10.1021/acsphotonics.5b00307

Yalcin A, Popat KC, Aldridge JC, et al., 2006. Optical sensing of biomolecules using microring resonators. *IEEE J Sel Top Quant*, 12(1):148-155. https://doi.org/10.1109/JSTQE.2005.863003

Yang Q, Wang WH, Xu S, et al., 2011. Enhancing light emission of ZnO microwire-based diodes by piezo-phototronic effect. *Nano Lett*, 11(9):4012-4017. https://doi.org/10.1021/nl202619d

Ymeti A, Kanger JS, Greve J, et al., 2003. Realization of a multichannel integrated Young interferometer chemical sensor. *Appl Opt*, 42(28):5649-5660. https://doi.org/10.1364/AO.42.005649

Yu L, Shi ZZ, Fang C, et al., 2015. Disposable lateral flow-through strip for smartphone-camera to quantitatively detect alkaline phosphatase activity in milk. *Biosens Bioelectron*, 69:307-315. https://doi.org/10.1016/j.bios.2015.02.035

Zenhausern F, Martin Y, Wickramasinghe HK, 1995. Scanning interferometric apertureless microscopy: optical imaging at 10 angstrom resolution. *Science*, 269(5227):1083-1085. https://doi.org/10.1126/science.269.5227.1083

Zhang JJ, Li GX, 2004. Third-generation biosensors based on the direct electron transfer of proteins. *Anal Sci*, 20(4):603-609. https://doi.org/10.2116/analsci.20.603

Zhang JL, Khan I, Zhang QW, et al., 2018. Lipopolysaccharides detection on a grating-coupled surface plasmon resonance smartphone biosensor. *Biosens Bioelectron*, 99:312-317. https://doi.org/10.1016/j.bios.2017.07.048

Zhu HY, Suter JD, White I, et al., 2006. Aptamer based microsphere biosensor for thrombin detection. *Sensors*, 6(8):785-795. https://doi.org/10.3390/s6080785

Zourob M, Goddard NJ, 2005. Metal clad leaky waveguides for chemical and biosensing applications. *Biosens Bioelectron*, 20(9):1718-1727. https://doi.org/10.1016/j.bios.2004.06.031

Zourob M, Mohr S, Brown BJ, et al., 2003a. The development of a metal clad leaky waveguide sensor for the detection of particles. *Sens Actuat B Chem*, 90:296-307. https://doi.org/10.1016/S0925-4005(03)00052-2

Zourob M, Mohr S, Fielden PR, et al., 2003b. Small-volume refractive index and fluorescence sensor for micro total analytical system (μ-TAS) applications. *Sens Actuat B Chem*, 94:304-312. https://doi.org/10.1016/S0925-4005(03)00460-X

Chen-lei PANG, first author of this invited paper, received his PhD degree in Optical Engineering in 2019 from Zhejiang University. He was awarded a scholarship under the State Scholarship Fund to study at California Institute of Technology as a joint PhD student from March 2018 to March 2019. He currently works at Zhejiang Lab, and his research interests focus on chip-based super-resolution imaging and defect inspection.

Qing YANG, corresponding author of this invited paper, received her BS and PhD degrees in College of Materials Science and Engineering from Zhejiang University in 2001 and 2006, respectively. She was a visiting scholar at Georgia Tech from 2009 to 2012, and a visiting scientist at University of Cambridge in 2018. She is currently a professor at the State Key Laboratory of Modern Optical Instrumentation, Zhejiang University, and an associate editor of *Science Bulletin*. Her research interests focus on smart and high-resolution sensing and imaging based on micro/nano-photonics.